

Model for the electrical conductivity in dense plasma mixtures

C. E. Starrett,^{1,*} N. R. Shaffer,¹ D. Saumon,¹ R. Perriot,¹ T. Nelson,¹ L. A. Collins,¹ and C. Ticknor¹

¹*Los Alamos National Laboratory, P.O. Box 1663, Los Alamos, NM 87545, U.S.A.*

(Dated: February 4, 2020)

A new model for the electrical conductivity of dense plasmas with a mixture of ion species, containing no adjustable parameters, is presented. The model takes the temperature, mass density and relative abundances of the species as input. It takes into account partial ionization, ionic structure, and core-valence orthogonality, and uses quantum mechanical calculations of cross sections. Comparison to an existing high fidelity but computationally expensive method reveals good agreement. The new model is computationally efficient and can reach high temperatures. A new mixing rule is also presented that gives reasonably accurate conductivities for high temperature plasma mixtures.

Keywords: electrical conductivity, mixtures, dense plasmas

I. INTRODUCTION

The calculation of the electrical conductivity of mixtures in the dense plasma regime is a difficult challenge that only a handful of studies have addressed. The issue is complicated by having to accurately model partial ionization, ionic structure, core-valence orthogonality, and a wide range of coupling strengths (between the ions and other ions, as well as between electrons and ions). The electrical conductivity of such plasmas, and the closely related thermal conductivity, are relevant to inertial and magneto-inertial fusion experiments [1, 2], as well as to white dwarf stars [3].

The ab initio method known as density functional theory molecular dynamics (DFT-MD), in conjunction with the Kubo-Greenwood formula [4–9], can be used to calculate the conductivity of mixtures for temperatures near or below the Fermi energy. This method uses few approximations but quickly becomes prohibitively expensive as temperature increases [10].

More approximate methods include the use of mixing rules to generate a mixture conductivity from pure (single ion species) plasma conductivities [11–13], but such an approach necessarily ignores cross-species correlations. Another approach is to treat the mixture as an effective single species [14, 15]. The early work of reference [16] used an extended Ziman formula with local pseudopotentials to calculate the conductivity of mixtures in the Born approximation with the Ziman approximation. The Ziman method is suited to highly degenerate electronic systems, which is not generally the case for plasmas. The Born approximation can lead to large errors in the conductivity for strong scatterers [17]. Other methods, such as the Zubarev generalized linear response method could be used to study the conductivity of mixtures [18, 19].

In this work we extend the previously developed potential of mean force method [20] to plasma mixtures. The extension introduces no additional approximations. We calculate the potential of mean force using the model of

reference [21], which is a DFT based average atom model that couples to the quantum Ornstein-Zernike equations. The cross sections are calculated using the quantum mechanical t-matrix method. We use the relaxation time approximation [22, 23] to calculate the conductivity, though the cross sections could be used in other kinetic theory approaches such as the Ziman method [24], or the Zubarev method [18]. We note that the use of the potential of mean force for transport was first developed in reference [25], for classical ionic transport coefficients.

Results from the model are compared to DFT-MD results for a range of mixtures, in particular to those relevant to inertial confinement fusion. The results are in generally good agreement and the model appears to be as accurate as the single species plasma model [20]. The model is numerically convenient, taking a few minutes on a single processor per point, and therefore is suitable for making data tables. A new conductivity mixing rule is also presented and compared to the model. The mixing rule takes the conductivity and average ionization of pure plasmas of each mixture species, at the same mass density and temperature, as input. Good agreement between the mixing rule and the potential for mean force model is found for high temperature plasmas.

The structure of this paper is as follows. In section II we review the quantum Ornstein-Zernike equations for mixtures, and introduce the potential of mean force, deriving it for mixtures. We also transform it into a numerically convenient and physically transparent form. In section III we give the equations to solve the relaxation time approximation for mixtures. In section IV numerical results are presented. These include comparisons to DFT-MD simulations for DT, BeDT and C₇H₉. The conductivity of asymmetric mixtures (high-Z with low-Z) is investigated and the accuracy of a Thomas-Fermi potential of mean force model is compared to the Kohn-Sham version. Finally in section V we present our conclusions. Throughout this work we use Hartree atomic units unless otherwise stated, in which $\hbar = m_e = k_B = e = 1$, where the symbols have their usual meaning.

*Electronic address: starrett@lanl.gov

II. POTENTIAL OF MEAN FORCE FOR MIXTURES

A. The potential of mean force

The potential of mean force $V_{ij}^{MF}(\mathbf{r})$ is the effective potential felt by a non-interacting particles such that the resulting particle density $n_j(\mathbf{r})$ is the same as in the interacting system [26]. For example, with classical particles the density distribution of species j around a central particle of species i can be written in the form [27]

$$n_j(\mathbf{r}) = n_j^0 \exp(-\beta V_{ij}^{MF}(\mathbf{r})) \quad (1)$$

and for quantal particles the expression is

$$n_e(\mathbf{r}) = \sum_j f(\epsilon_j) |\phi_j(\mathbf{r})|^2 \quad (2)$$

where $f(\epsilon_j)$ is the Fermi-Dirac function, $\phi_j(\mathbf{r})$ is the wave function that satisfies the Schrödinger equation with potential $V_{ie}^{MF}(\mathbf{r})$, and the sum is over all eigenstates.

To derive an expression for $V_{ij}^{MF}(r)$, we note that if F^{ex} is the excess free energy of the system, then the Euler equations [28] give

$$V_{ij}^{MF}(\mathbf{r}) = V_{ij}(r) + \frac{\delta F^{ex}}{\delta n_i(\mathbf{r})} - \mu_i^{ex} \quad (3)$$

where μ_i^{ex} is the excess chemical potential of species i and $V_{ij}(r)$ is the pair interaction potential. By using a functional Taylor expansion of the excess free energy F^{ex} about a uniform reference system, an expression for the potential of mean force $V_{ij}^{MF}(r)$ of an isotropic system can be found [28, 29]

$$V_{ij}^{MF}(r) = V_{ij}(r) + \sum_{\lambda=1}^{N+1} n_{\lambda}^0 \int d^3r' \frac{C_{\lambda j}(|\mathbf{r} - \mathbf{r}'|)}{-\beta} h_{i\lambda}(r') \quad (4)$$

where the direct correlation function is related to the second functional derivative of the excess free energy

$$C_{ij}(|\mathbf{r} - \mathbf{r}'|) = -\beta \frac{\delta^2 F^{ex}}{\delta n_i(\mathbf{r}) \delta n_j(\mathbf{r}')} \quad (5)$$

For classical ions of charge \bar{Z}_i and \bar{Z}_j , $V_{ij}(r) = \bar{Z}_i \bar{Z}_j / r$. For quantal electrons interacting with an ion of species i , $V_{ie}(r) = -\bar{Z}_i / r$ if we assume a point ion. However, we define an ion as a point nucleus with bound electrons,

$$V_{ie}(r) = -\frac{Z_i}{r} + \int d^3r' \frac{n_{i,e}^{ion}(r')}{|\mathbf{r} - \mathbf{r}'|} + V^{xc}[n_{i,e}^{ion}(r)] \quad (6)$$

where $n_{i,e}^{ion}(r)$ is the electron density of the bound electrons around ion i and V^{xc} is the exchange and correlation potential.

Implicit in equation (4) is the neglect of expansion terms beyond second order. For classical particles these higher order terms are often collected together in the so-called bridge function [27, 30]. Neglect of these terms corresponds the Hyper-Netted Chain (HNC) approximation [31].

B. Quantum Ornstein-Zernike equations

The quantum Ornstein-Zernike (QOZ) equations [32] for a mixture of quantal electrons and N classical ion species were derived in reference [21]

$$h_{ij}(k) = \left(-\frac{\chi_{jj}^0(k)}{\beta n_j^0} \right) \left[C_{ij}(k) + \sum_{\lambda=1}^{N+1} n_{\lambda}^0 h_{i\lambda}(k) C_{\lambda j}(k) \right] \quad (7)$$

where $h_{ij}(k)$ is the total correlation function in Fourier space ($h_{ij}(r) = g_{ij}(r) - 1$, where $g_{ij}(r)$ is the pair distribution function), $C_{ij}(k)$ is the direct correlation function, and $\chi_{jj}^0(k)$ is the non-interacting response function. For classical particles $\chi_{jj}^0/\beta n_j^0 = 1$, where n_j^0 is the average particle density for species j and β is the inverse of the temperature. For the quantal electrons χ_{ee}^0 is the finite-temperature Lindhard function [33]. Equation (7) is valid if at least one of the species is classical. For the electron-electron pair distribution function, see reference [34].

To solve the QOZ equations we map them to a system of N classical ions screened by electrons, where the screening density for species i is

$$n_{i,e}^{scr}(k) = -\frac{C_{ie}(k)}{\beta} \chi'_{ee}(k) \quad (8)$$

with

$$\chi'_{ee}(k) \equiv \frac{\chi_{ee}^0(k)}{1 + \chi_{ee}^0(k) C_{ee}(k) / \beta} \quad (9)$$

This mapping leads to the N -component classical OZ equations with HNC closure relations [26]

$$h_{IJ}(k) = C_{IJ}(k) + \sum_{\lambda=1}^N n_{\lambda}^0 h_{I\lambda}(k) C_{\lambda J}(k) \quad (10)$$

$$h_{IJ}(r) + 1 = \exp(-\beta V_{IJ}(r) + h_{IJ}(r) - C_{IJ}(r)) \quad (11)$$

where the ion-ion pair interaction potentials are given by

$$V_{IJ}(k) = \frac{4\pi \bar{Z}_i \bar{Z}_j}{k^2} - \frac{C_{ie}(k)}{\beta} n_{j,e}^{scr}(k). \quad (12)$$

Here, screened ion I (J) corresponds to ion i (j) in the full QOZ equations. These pair potentials, equation (12), are the interaction potentials for pairs of ‘dressed’ ions, defined by a point charge \bar{Z}_j and a neutralizing, screening electron cloud $n_{j,e}^{scr}(r)$. In the limit of high temperatures equation (12) reduces to a Debye-Hückel potential with the screening length given by the electron Debye length.

The screening densities are provided by finite temperature density functional theory [6] average atom calculations [21]. One can view these screening densities as electron-ion closure relations. The closure relation for the electron-electron direct correlation function C_{ee} is provided by the jellium model, with the local field correction provided by reference [35]. With these closure relations we can solve the QOZ's for the correlation functions h_{ij} and C_{ij} .

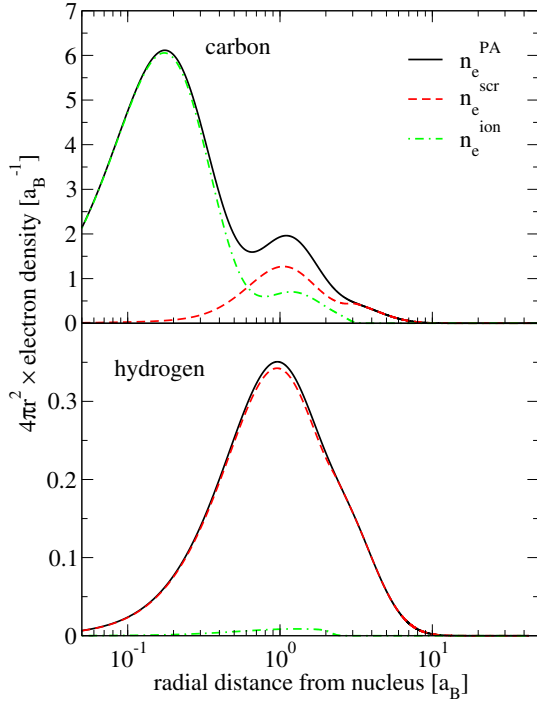


FIG. 1: (Color online) Example of pseudoatom, screening and ion densities for an equi-molar carbon-hydrogen mixture at 1 g/cm³ and 10 eV temperature. For carbon, average ionization per atom is $\bar{Z}_C = 3.01$, for hydrogen it is $\bar{Z}_H = 0.986$.

C. Electron-ion potential of mean force

Equation (4) is valid as long as at least one species is classical [29, 34]. The electron-ion potential of mean force is then

$$V_{ie}^{MF}(r) = V_{ie}(r) + \sum_{\lambda=1}^N n_{\lambda}^0 \int d^3r' \frac{C_{\lambda e}(|\mathbf{r} - \mathbf{r}'|)}{-\beta} h_{i\lambda}(r') + \bar{n}_e^0 \int d^3r' \frac{C_{ee}(|\mathbf{r} - \mathbf{r}'|)}{-\beta} h_{ie}(r') \quad (13)$$

Setting $N = 1$ recovers the single species result, equation (26) of reference [20]. This potential can be rewritten as a sum of Hartree, ion-ion and ion-electron correlation, and electron-electron exchange and correlation terms. First note that the QOZ equations give

$$\bar{n}_e^0 h_{ie}(k) = n_{i,e}^{scr}(k) + \sum_{\lambda=1}^N n_{\lambda}^0 h_{i\lambda}(k) n_{\lambda,e}^{scr}(k) \quad (14)$$

Now define

$$n_{i,e}^x(k) = \sum_{\lambda=1}^N n_{\lambda}^0 h_{i\lambda}(k) n_{\lambda,e}^{scr}(k) \quad (15)$$

which is the density of electrons surrounding the non-central ions, then

$$\bar{n}_e^0 h_{ie}(k) = n_{i,e}^{scr}(k) + n_{i,e}^x(k) \quad (16)$$

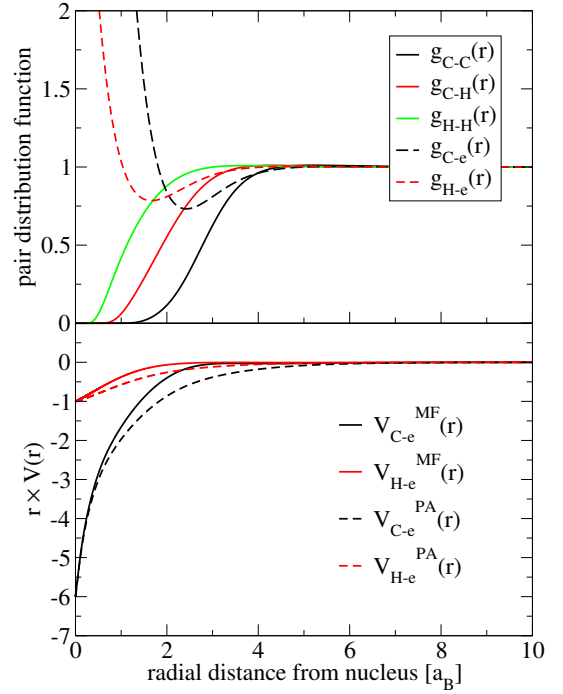


FIG. 2: (Color online) Example of ion-ion and ion-electron pair distribution functions (top panel) for an equi-molar carbon-hydrogen mixture at 1 g/cm³ and 10 eV temperature. The bottom panel shows the potentials $V^{MF}(r)$ and $V^{PA}(r)$ for the same case. The difference is the contribution to screening from the other ions and their screening electrons.

Using this together with

$$C_{ij}(k) = -\beta V_{ij}^C(k) + \tilde{C}_{ij}(k) \quad (17)$$

where $\tilde{C}_{ij}(k)$ contains the correlation contribution (and exchange for \tilde{C}_{ee}), and V_{ij}^C is the Coulomb pair potential, then

$$V_{ie}^{MF}(r) = V_i^{PA}(r) + \int d^3r' \frac{\sum_{\lambda=1}^N -n_{\lambda}^0 \bar{Z}_{\lambda} h_{\lambda i}(r') + n_{i,e}^x(r')}{|\mathbf{r} - \mathbf{r}'|} + V^{xc}[n_{i,e}^x(r) + \bar{n}_e^0] - V^{xc}[\bar{n}_e^0] + \sum_{\lambda=1}^N n_{\lambda}^0 \int d^3r' \frac{\tilde{C}_{\lambda e}(|\mathbf{r} - \mathbf{r}'|)}{-\beta} h_{i\lambda}(r') \quad (18)$$

Here

$$V_i^{PA}(r) = -\frac{Z_i}{r} + \int d^3r' \frac{n_{i,e}^{PA}(r')}{|\mathbf{r} - \mathbf{r}'|} + V^{xc}[n_{i,e}^{PA}(r)] \quad (19)$$

is the pseudoatom potential and

$$n_{i,e}^{PA}(r) = n_{i,e}^{ion}(r) + n_{i,e}^{scr}(r). \quad (20)$$

is the pseudoatom density, which here is provided by the average atom model [21]. The pseudoatom is defined by

the nucleus and the electrons that screen it, including bound and conduction electrons. The second term in equation (18) is Hartree-Coulomb interactions between the ions surrounding the central pseudoatom, and the electrons surrounding these ions ($n_{i,e}^x$). The third and fourth terms are the exchange and correlation interactions of these electrons. The fifth term is due to electron-ion correlations.

An example of pseudoatom, screening (conduction) and ion (bound) densities are shown in figure 1. For the same case, the pair distribution functions and potentials of mean force are shown in figure 2. The peaks in the carbon pseudoatom density in figure 1 are due to the shell structure; the peak near $0.2 a_B$ is due to electrons in the $1s$ orbital, the peak near $1 a_B$ is due to electrons in the $2s$ orbital. The tail of the electron density is due to the ionized electrons. For hydrogen, the $1s$ state is weakly bound $\epsilon_{1s} = -0.0042 E_h$ and is nearly fully depopulated, leading to a small bound electron density around each hydrogen nucleus $n_{i,e}^{ion}(r)$ (figure 1). The ionized electrons form the screening density which dominates the pseudoatom density.

In the top panel of figure 2, the ion-electron pair distribution functions for carbon and hydrogen reflect the smaller size and charge of the hydrogen ion. This feeds into the ion-ion pair distribution functions, where the Coulomb hole, due to repulsion of the ions to each other at small separations, is smaller for H-H than for C-C distributions, with C-H lying in between. The lack of oscillations in the ion-ion pair distribution functions indicates a moderately coupled ionic fluid, as expected under these conditions. The bottom panel of the figure shows the ion-electron potentials of mean force compared to the pseudoatom potentials. The effect of including the screening from the other ions is to weaken the effective scattering potential, i.e. make the effective screening length shorter.

III. ELECTRICAL CONDUCTIVITY WITH THE RELAXATION TIME APPROXIMATION

We calculate the electrical conductivity of the plasma using the relaxation time approximation [22, 23].

$$\sigma_{DC} = \frac{1}{3\pi^2} \int_0^\infty \left(-\frac{df(\epsilon, \mu)}{d\epsilon} \right) v^3 \tau_\epsilon d\epsilon \quad (21)$$

where $f(\epsilon, \mu)$ is the Fermi-Dirac occupation factor, ϵ the electron energy $\epsilon = mv^2/2$, μ is the electron chemical potential and τ_ϵ is the relaxation time. Using Matthiessen's rule, which assumes that scattering mechanisms are independent [36], τ_ϵ is calculated from the relaxation time due to each species [37]

$$\frac{1}{\tau_\epsilon} = \sum_{i=1}^N \frac{1}{\tau_{i,\epsilon}} \quad (22)$$

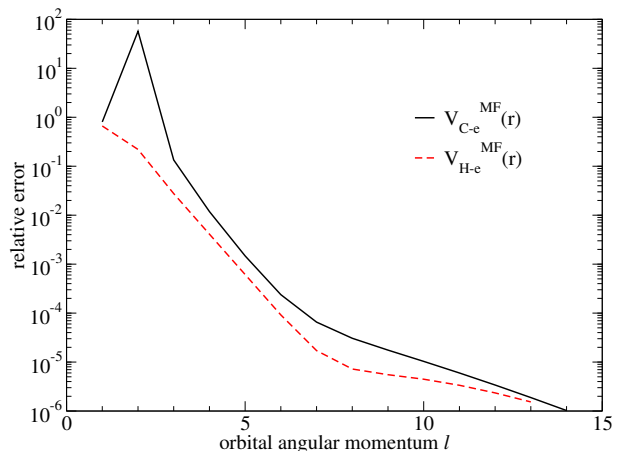


FIG. 3: (Color online) Convergence of the conductivity with respect to the maximum orbital angular momentum for the sum in equation (24), for an equi-molar carbon-hydrogen mixture at 1 g/cm^3 and 10 eV temperature. We converge on the relative error in the effective conductivity for each species, hence the two lines. More degenerate plasmas should converge faster, while more weakly degenerate cases will converge more slowly, for $l > 30$ we use a semi-classical calculation of the phase shifts [20] for computational efficiency.

where the relaxation times are calculated from the momentum transport cross sections

$$\tau_{i,\epsilon} = \frac{1}{n_i^0 v \sigma_{i,\text{tr}}(\epsilon)} \quad (23)$$

The momentum transport cross section is calculated by solving the Schrödinger equation for the phase shifts $\eta_l(\epsilon)$ due to the scattering potential $V_{ie}^{MF}(r)$

$$\sigma_{i,\text{tr}}(\epsilon) = \frac{4\pi}{v^2} \sum_{l=0}^{\infty} (l+1) (\sin(\eta_{l+1} - \eta_l))^2 \quad (24)$$

where the sum over orbital angular momentum quantum number l converges, see figure 3. In the figure we show the relative change in the effective one-species conductivity caused by adding another term to the l summation in equation (24). The effect of electron-electron collisions is modeled using the fit formula of reference [38].

We note that equations (21) and (22) cannot be decomposed (without approximation) into a simple sum of single species conductivities, as one would have in a mixing rule, for example [11].

IV. NUMERICAL RESULTS

A. Comparison to DFT-MD simulations

In figure 4 we compare results from the present model to DFT-MD simulations that used the Kubo-Greenwood approximation to evaluate the transport properties [11,

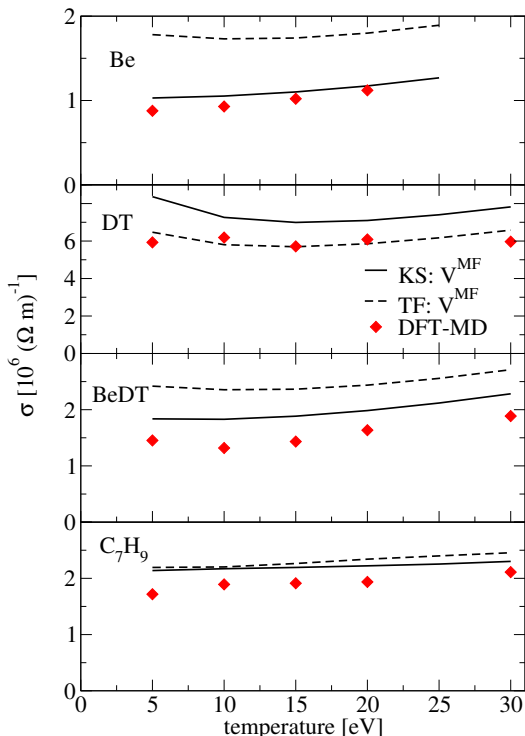


FIG. 4: (Color online) Results from the present model V^{MF} in the Thomas-Fermi (TF) or Kohn-sham (KS) approximation, compared to DFT-MD simulations using the Kubo-Greenwood approximation [11, 39]. In all cases the density is 10 g/cm^3 . The Fermi temperature for Be is 44.3 eV , for DT 65.0 eV , for BeDT 51.7 eV , and for CH 65.0 eV .

39]. Our calculations use either the potential of mean force calculated using the semi-classical, orbital free, Thomas-Fermi (TF) version of the model presented in reference [21], or the less approximate Kohn-Sham version (KS). In all cases we have used the temperature dependent exchange and correlation potential of reference [40]. In the caption we also give the Fermi temperature T_F for each case (using the KS ionization value). This depends very weakly on temperature (via the ionization) so we give the average value for the conditions plotted. For all cases the temperature is much less than T_F indicating a degenerate plasma.

From figure 4 we see reasonably good agreement of the present model with the DFT-MD calculations. In physical content these DFT-MD simulations are more complete than the present model and therefore should be more accurate. They are however, expensive in terms of computational cost and can have issues with numerical convergence [41, 42]. This computational cost limitation becomes increasingly acute for temperatures above the Fermi energy. For all cases except the DT mixture, the KS version of the model is in better agreement with the DFT-MD than the TF version, as expected, as it is a less approximate method. The exception, DT is further examined in figure 5. There we compare to Kubo-

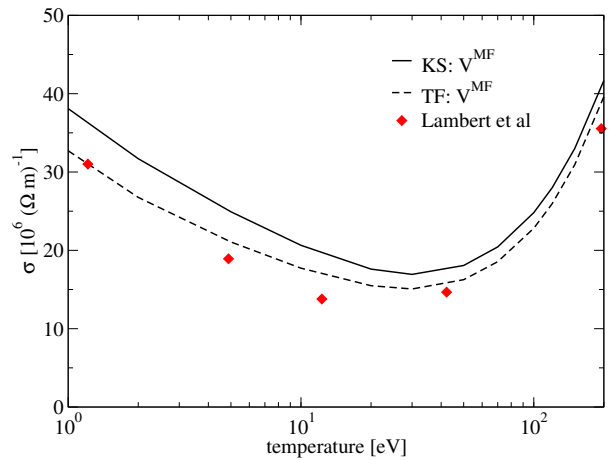


FIG. 5: (Color online) Results from the present model compared to the Kubo-Greenwood DFT-MD results of reference [41] for dense hydrogen at 10 g/cm^3 .

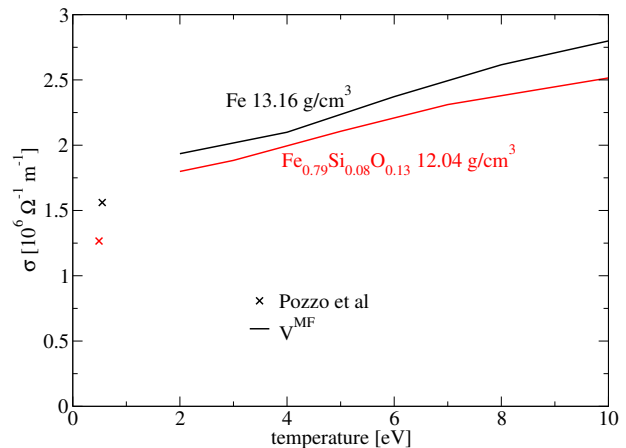


FIG. 6: (Color online) Comparison of the present model to the Kubo-Greenwood DFT-MD calculations of reference [43]. We use the KS version of our model.

Greenwood DFT-MD results for pure hydrogen at 10 g/cm^3 as a function of temperature. Again we see that the TF version of the model is in closer agreement with the DFT-MD results. We have no definite explanation of this, but believe it just fortuitous. The KS version overestimates the conductivity in these cases, where $\bar{Z} = 1$ is predicted and is expected. The error is reduced in the TF version because $\bar{Z} < 1$ due to the lack of shell structure. Hence, a cancellation of errors may be occurring for the TF version. For Be, figure 4, TF overestimates the conductivity and also predicts a larger average ionization ~ 2.7 , versus ~ 2.0 for KS, so this is consistent. We also note that good agreement of the present model with DFT-MD simulations for the electrical conductivity of hydrogen plasmas, at 40 g/cm^3 and temperatures from 500 to 900 eV , was found in reference [20].

In figure 6 we compare to DFT-MD results for pure

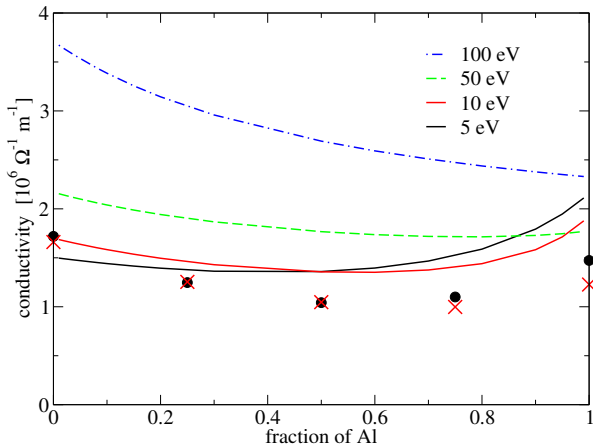


FIG. 7: (Color online) Conductivity of aluminum-carbon mixture at 10 g/cm^3 . Lines are from the present model, symbols are Kubo-Greenwood DFT-MD results (filled circles 5 eV, crosses 10 eV).

Fe and for a Fe mixture relevant to the Earth’s interior [43]. We were unable to obtain reliable results at the same temperature as the DFT-MD results. This is due to a breakdown of a number of approximations in the model. On the one hand the average atom itself is inaccurate under these conditions due to the free electron boundary conditions on the atom, whereas for iron, multiple scattering, which is ignored here, is strong [44]. Also, to solve the QOZ equations (and to use the kinetic theory model), a definition of an ion is required. This is difficult to do unambiguously due to the large iron $3d$ resonance state in the continuum of free electrons. Moreover, use of the relaxation time approximation (21) assumes a binary collision approximation, which becomes an unsafe assumption for resonance states, as evidenced by the strong multiple scattering effect [44]. All these effects conspire to mean the model is unreasonable for dense iron at temperatures below $\sim 2 \text{ eV}$. In contrast, for aluminum [45], we found reasonable results to 0.2 eV at solid density, where none of the above problems are relevant. Nevertheless, the trend seen in figure 6, of a reduced conductivity for the mixture, is reproduced and the absolute numbers are reasonable.

In figure 7 we compare the present model to Kubo-Greenwood DFT-MD simulations for an aluminum-carbon mixture at 10 g/cm^3 (see appendix B for details of our DFT-MD simulations). The level of agreement is reasonable at both 5 and 10 eV, and is similar to what we have seen in figures 4 to 6. Interestingly, for the two lowest temperatures a minimum in the conductivity is observed as a function of the fraction of aluminum in both the model and DFT-MD results. This is reminiscent of Nordheim’s rule for alloys [36]. The conductivity decreases as the ‘impurity’ is added starting for either pure phase. Faber and Ziman explained

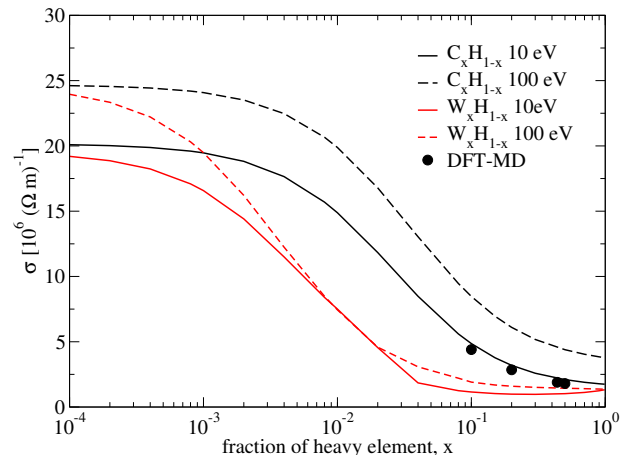


FIG. 8: (Color online) Electrical conductivity of high-Z, low-Z mixtures at 10 g/cm^3 as a function of the fraction of the heavy element. We have used the KS version of the model. Also shown are DFT-MD Kubo-Greenwood calculations for C_xH_{1-x} at 10 eV. These are extensions of the calculations of reference [11].

this behavior as being due to cross-terms in the scattering amplitudes [46]. These cross-terms are important if structure factors $S_{ij}(k)$ are significantly different from unity at relevant electronic wave numbers k . These relevant wave numbers are determined by the range of values for which derivative of the Fermi occupation factor is different from zero. In degenerate cases only the Fermi wave number k_F is relevant, and the $S_{ij}(k_F)$ typically differ from unity. At higher temperature, larger k ’s are relevant where $S_{ij}(k) \rightarrow 1$ so the conductivity changes monotonically, as the cross-terms are negligible. Physically, the minimum for more degenerate systems is related to a reduction in coherent scattering due to the presence of impurities. At the higher temperatures coherent scattering is disrupted by thermal ionic disorder. For the two highest temperatures plotted in figure 7, the drop in conductivity on increasing aluminum fraction is mainly due to a decrease in the average ionization.

Overall, the level of agreement seen in figures 4 to 7 indicates that the mixture and the single species models are of similar accuracy, relative to Kubo-Greenwood DFT-MD. We expect the predictions to become more accurate as temperature increases and the model will eventually recover the Debye-Hückle limit [47].

B. Applications of the model

Next we look at two applications of the model. In figure 8 we show the conductivity of C_xH_{1-x} and W_xH_{1-x} as a function of x for plasmas at 10 g/cm^3 . Also shown are DFT-MD Kubo-Greenwood calculations for C_xH_{1-x} at 10 eV. These are new calculations but are essentially extensions of the calculations presented in reference

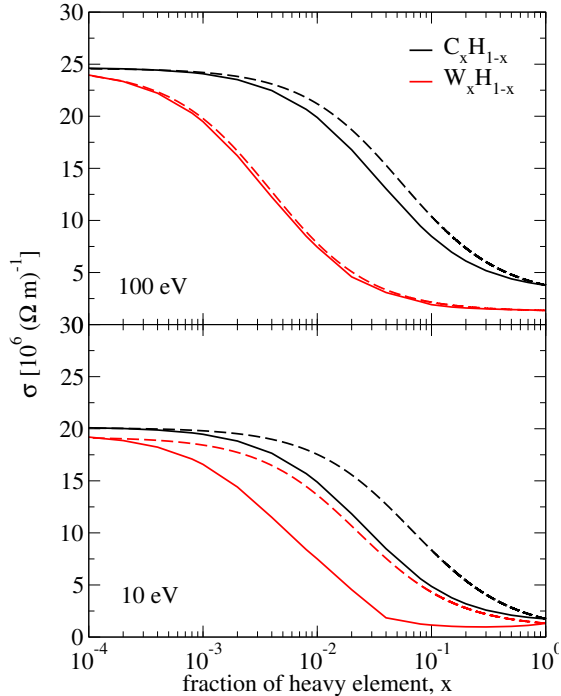


FIG. 9: (Color online) Solid lines: the result from the KS version of the model, as in figure 8. Dashed lines: the new mixing rule equation (25). Top panel, results at a temperature of 100 eV; bottom panel, results at 10 eV. The mixing rule works better at high temperature, as expected.

[11, 39]. Good agreement is observed. We note that it becomes impractical to use DFT-MD for mixtures where one element is a trace due to the need for at least one atom of the trace species to be in the computational supercell, and preferably more than one atom to reduce statistical noise. The main result of figure 8 is a highly asymmetrical transition between the single species plasmas, with the asymmetry being more pronounced for the higher- Z mixture. This behavior can be understood by considering the following mixing rule (which is described in appendix A)

$$\sigma_{DC} = \sum_{i=1}^N Y_i \sigma_{i,DC} \quad (25)$$

where $\sigma_{i,DC}$ is the conductivity of a pure (single ion species) plasma of species i , and the coefficients Y_i are

$$Y_i = x_i \frac{(\bar{Z}_i^p)^2}{\sum_{j=1}^N x_j (\bar{Z}_j^p)^2} \quad (26)$$

This mixing rule takes the conductivities ($\sigma_{i,DC}$) and average ionizations \bar{Z}_i^p of pure (indicated by superscript p)

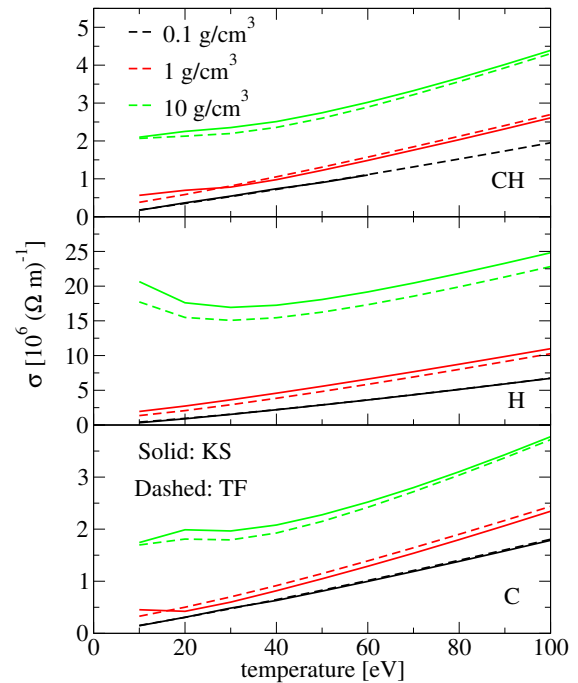


FIG. 10: (Color online) Comparison of the TF and KS versions of the model for CH, H and C plasmas for 0.1, 1, and 10 g/cm³, from 10 through 100 eV. The TF and KS models agree best for non-degenerate cases.

plasmas of the mixture components (at the same mass density and temperature), and generates the mixture conductivity σ_{DC} .

In figure 9 we show the result of this new mixing rule for CH and WH plasmas. We see that the trends are well reproduced telling us that the asymmetrical behaviour can be understood as the weighted mixing of large and small ion charges. The mixing rule will become inaccurate for lower temperatures, and figure 9 confirms this. This is in part due to the breakdown of the assumed Coulomb logarithm form (appendix A). The model (equation (25)) offers a rapid and reasonably accurate method of estimating the conductivity of plasma mixtures from the pure plasma conductivities. Another point worth noting is that the mixing rule predicts that the larger the charge asymmetry, the smaller the amount of the more highly charged ion is needed to have a significant effect on the mixture conductivity.

The second application of the model is to evaluate the Thomas-Fermi model through comparison with the Kohn-Sham version. Note that in both the TF and KS versions the cross section is evaluated quantum mechanically using equation (24), only the generation of V_{ie}^{MF} changes. In figure 10 we compare these for a CH mixture and for pure hydrogen and carbon plasmas. The agreement between the TF and KS versions improves for lower density and higher temperatures, i.e. for lower degeneracy plasmas. Since the derivative of the Fermi-Dirac

function is broader for lower degeneracy, the energy integral in equation (21) has a wider range of energies that are significant, including higher energies where the TF cross section is a better approximation to KS. The result will be therefore less sensitive to the details of the relaxation time, hence use of the TF $V^{MF}(r)$ should be more reasonable. We note also that the TF model is just as accurate for the mixture as it is for the pure hydrogen and carbon plasmas (compared to the KS model).

V. CONCLUSIONS

A model for calculating the conductivity of dense plasma mixtures has been presented. The model is an extension to multicomponent ionic mixtures of the model presented in reference [20], and builds on the multicomponent electronic and ionic structure model presented in reference [21]. The new conductivity model is computationally efficient, taking a few minutes per density and temperature point. It can also reach temperatures much higher than the Fermi energy, in contrast to other methods based on DFT [39, 41, 42].

We have evaluated the new model by comparing it to DFT-MD simulations that use the Kubo-Greenwood approximation. The model is in reasonably good agreement with these less approximate results for a variety of physical plasmas.

The conductivity of asymmetric mixtures (high-Z, low-Z) was investigated with a newly proposed mixing rule. This model predicts that the ion charge asymmetry is what drives the change in the conductivity, and that the higher the charge asymmetry, the less of the highly charged ion is needed to have a significant effect. The mixing rule is expected to work best for high temperatures, and represents a simple and rapid way to obtain reasonably accurate mixture conductivities from the pure plasma conductivities and average ionizations.

Finally, it was found that using a Thomas-Fermi model for the potential of mean force gave good agreement with the Kohn-Sham version for sufficiently high temperature or low density.

Acknowledgments

This work was performed under the auspices of the United States Department of Energy under contract 89233218CNA000001.

Appendix A: Mixing rule

In this appendix we show how we arrive at the new mixing rule, equation (25), which aims to estimate the mixture conductivity from the pure plasma conductivities of the components, at the same mass density and temperature. Following reference [37], the momentum

transport cross section can be approximated in terms of a Coulomb logarithm ($\log \Lambda$)

$$\sigma_{i,\text{tr}}(\epsilon) = \frac{4\pi e^4 \bar{Z}_i^2 \log \Lambda_i}{m^2 v^4} \quad (\text{A1})$$

Making the ansatz

$$\sigma_{DC} = \sum_{i=1}^N Y_i \sigma_{i,DC} \quad (\text{A2})$$

where Y_i are coefficients, and $\sigma_{i,DC}$ are the conductivities for pure plasmas of species i only (at the same mass density and temperature as the mixture), and using equation (21) and (22), we have

$$1 = \sum_{i=1}^N Y_i \frac{\sum_{j=1}^N n_j^0 \bar{Z}_j^2 \log \Lambda_j F(\mu)}{n_i^{0,p} (\bar{Z}_i^p)^2 \log \Lambda_i^p F(\mu_i^p)} \quad (\text{A3})$$

On the top line, the quantities with subscript j refer to properties of ions in the mixture, and on the bottom line, quantities with a superscript p refer to pure plasma properties, and

$$F(\mu) = \frac{2}{\pi^3} \int_0^\infty d\epsilon \epsilon^3 f(\mu) \quad (\text{A4})$$

Equation (A3) is satisfied if we choose

$$Y_i = x_i \frac{n_i^{0,p} (\bar{Z}_i^p)^2 \log \Lambda_i^p F(\mu_i^p)}{\sum_{j=1}^N n_j^0 \bar{Z}_j^2 \log \Lambda_j F(\mu)} \quad (\text{A5})$$

which we can approximate as

$$Y_i \approx x_i \frac{(\bar{Z}_i^p)^2}{\sum_{j=1}^N x_j (\bar{Z}_j^p)^2} \quad (\text{A6})$$

This assumes that

$$\frac{n_j^0}{n_i^{0,p}} \approx \frac{n_j^0}{n_I^0} = x_j, \quad (\text{A7})$$

$$\frac{\log \Lambda_j F(\mu)}{\log \Lambda_i^p F(\mu_i^p)} \approx 1 \quad (\text{A8})$$

and finally

$$\bar{Z}_i \approx \bar{Z}_i^p \quad (\text{A9})$$

Appendix B: DFT-MD simulations

We have performed DFT-MD calculations with the Vienna ab-initio simulation package (VASP [48–51]), using the Generalized Gradient Approximation – Perdew,

TABLE I: DFT-MD σ_{DC} results for $C_x\text{-Al}_{1-x}$ at 10 g/cm^3 in units of $10^6 \Omega^{-1} \text{ m}^{-1}$.

| | Temperature [eV] | |
|----------------------|------------------|-------|
| | 5 | 10 |
| Carbon fraction, x | | |
| 0 | 1.473 | 1.227 |
| 0.25 | 1.1 | 0.998 |
| 0.5 | 1.042 | 1.047 |
| 0.75 | 1.267 | 1.254 |
| 1 | 1.719 | 1.661 |

Burke, Ernzerhof for the XC functional (GGA-PBE [51, 52]). We employed the GW $3e^-$ plane augmented wave (PAW) pseudopotential (PP) for Al, and the $4e^-$ PAW

PP for C [53, 54], with a planewave cutoff energy of 750 eV. The DFT-MD simulations were performed at constant temperature using the Nose-Hoover thermostat and a timestep of 1 fs.

We followed the procedure validated for pure Al in the WDM regime, and discussed in a recent publication [55]. Pre-molten samples containing 64 atoms at density ρ were first equilibrated at temperature T for at least 2 ps. From this run, ten snapshots separated by 50 fs were used to calculate the DC conductivity via optical analysis. The MD stage calculations were performed at the Gamma-point, while a $2 \times 2 \times 2$ k-point mesh (generating 4 independent k-points) was used for the optical analysis. We imposed a number of bands N during the MD such that the maximum occupation of the highest band is less than 1×10^{-4} , and used $2N$ bands for the optical analysis.

Regarding the C-H calculations, which are extensions of the calculations of reference [11], we also used PBE-PAW PP, with a cutoff energy of 700 eV. Simulation cells containing 128 to 250 atoms were tested, yielding results differing by at most 10% (for the C-90%/H-10% case). All calculations were performed at the Γ -point.

-
- [1] Matthew R. Gomez, Stephen A. Slutz, Adam B. Sefkow, Daniel B. Sinars, Kelly D. Hahn, Stephanie B. Hansen, Eric C. Harding, Patrick F. Knapp, Paul F. Schmit, Christopher A. Jennings, et al. Experimental demonstration of fusion-relevant conditions in magnetized liner inertial fusion. *Physical review letters*, 113(15):155003, 2014.
- [2] Hans G. Rinderknecht, P.A. Amendt, S.C. Wilks, and G. Collins. Kinetic physics in ICF: present understanding and future directions. *Plasma Physics and Controlled Fusion*, 60(6):064001, 2018.
- [3] Robert Eugene Marshak. The internal temperature of white dwarf stars. *The Astrophysical Journal*, 92:321, 1940.
- [4] W. Kohn and L. J. Sham. Self-consistent equations including exchange and correlation effects. *Phys. Rev.*, 140:A1133–A1138, Nov 1965.
- [5] P. Hohenberg and W. Kohn. Inhomogeneous electron gas. *Phys. Rev.*, 136:B864–B871, Nov 1964.
- [6] N. David Mermin. Thermal properties of the inhomogeneous electron gas. *Phys. Rev.*, 137:A1441–A1443, Mar 1965.
- [7] D.A. Greenwood. The boltzmann equation in the theory of electrical conduction in metals. *Proceedings of the Physical Society*, 71(4):585, 1958.
- [8] M. P. Desjarlais, J. D. Kress, and L. A. Collins. Electrical conductivity for warm, dense aluminum plasmas and liquids. *Phys. Rev. E*, 66:025401, Aug 2002.
- [9] S.X. Hu, V.N. Goncharov, T.R. Boehly, R.L. McCrory, S. Skupsky, Lee A. Collins, Joel David Kress, and B. Militzer. Impact of first-principles properties of deuterium-tritium on inertial confinement fusion target designs. *Physics of Plasmas*, 22(5):056304, 2015.
- [10] Travis Sjoström and Jérôme Daligault. Ionic and elec-

TABLE II: DFT-MD σ_{DC} results for $C_x\text{-H}_{1-x}$ at 10 g/cm^3 in units of $10^6 \Omega^{-1} \text{ m}^{-1}$.

| | | Temperature [eV] |
|----------------------|--------|------------------|
| | | 10 |
| Carbon fraction, x | 0.1 | 4.4 |
| | 0.2 | 2.85 |
| | 0.4375 | 1.89 |
| | 0.5 | 1.8 |

tronic transport properties in dense plasmas by orbital-free density functional theory. *Phys. Rev. E*, 92:063304, 2015.

- [11] C. E. Starrett, J Cl erouin, V Recoules, J. D. Kress, L. A. Collins, and D. E. Hanson. Average atom transport properties for pure and mixed species in the hot and warm dense matter regimes. *Physics of Plasmas (1994-present)*, 19(10):102709, 2012.
- [12] W.R. Johnson, C. Guet, and G.F. Bertsch. Optical properties of plasmas based on an average-atom model. *Journal of Quantitative Spectroscopy and Radiative Transfer*, 99(13):327 – 340, 2006. Radiative Properties of Hot Dense Matter.
- [13] M. Yu. Kuchiev and W. R. Johnson. Low-frequency

- plasma conductivity in the average-atom approximation. *Phys. Rev. E*, 78:026401, Aug 2008.
- [14] G. Faussurier, C. Blancard, P. Combis, and L. Videau. Electrical and thermal conductivities in dense plasmas. *Physics of Plasmas (1994-present)*, 21(9):092706, 2014.
- [15] R. M. More, K. H. Warren, D. A. Young, and G. B. Zimmerman. A new quotidian equation of state (qeos) for hot dense matter. *The Physics of Fluids*, 31(10):3059–3078, 1988.
- [16] F. Perrot and M.W.C. Dharma-Wardana. Equation of state and transport properties of an interacting multispecies plasma: Application to a multiply ionized al plasma. *Physical Review E*, 52(5):5352, 1995.
- [17] D.J. Burrill, D.V. Feinblum, M.R.J. Charest, and C.E. Starrett. Comparison of electron transport calculations in warm dense matter using the Ziman formula. *High Energy Density Physics*, 19:1 – 10, 2016.
- [18] D. N. Zubarev. Nonequilibrium statistical thermodynamics. *Nonequilibrium statistical thermodynamics*, 1973.
- [19] Ronald Redmer. Electrical conductivity of dense metal plasmas. *Phys. Rev. E*, 59:1073–1081, Jan 1999.
- [20] C.E. Starrett. Potential of mean force for electrical conductivity of dense plasmas. *High Energy Density Physics*, 25:8 – 14, 2017.
- [21] C. E. Starrett, D. Saumon, J. Daligault, and S. Hamel. Integral equation model for warm and hot dense mixtures. *Physical Review E*, 90(3):033110, 2014.
- [22] P. L. Bhatnagar, E. P. Gross, and M. Krook. A model for collision processes in gases. i. Small amplitude processes in charged and neutral one-component systems. *Phys. Rev.*, 94:511–525, May 1954.
- [23] Nicholas A. Krall and Alvin W. Trivelpiece. *Principles of Plasma Physics*. New York, :McGraw-Hill, 1973.
- [24] John M. Ziman. *Electrons and phonons: the theory of transport phenomena in solids*. Oxford University Press, 1960.
- [25] Scott D. Baalrud and Jérôme Daligault. Effective potential theory for transport coefficients across coupling regimes. *Phys. Rev. Lett.*, 110:235001, Jun 2013.
- [26] J. K. Percus. Approximation methods in classical statistical mechanics. *Phys. Rev. Lett.*, 8:462–463, Jun 1962.
- [27] J.-P. Hansen and I.R. McDonald. *Theory of simple liquids, Third edition*. Academic Press, 2006.
- [28] J. A. Anta and A. A. Louis. Probing ion-ion and electron-ion correlations in liquid metals within the quantum hypernetted chain approximation. *Phys. Rev. B*, 61:11400–11410, May 2000.
- [29] A. A. Louis, H. Xu, and J. A. Anta. Combining quantum and classical density functional theory for ion–electron mixtures. *Journal of non-crystalline solids*, 312:60–68, 2002.
- [30] Hiroshi Iyetomi and Setsuo Ichimaru. Improvement on the hypernetted-chain equations for dense plasmas. *Phys. Rev. A*, 25:2434–2436, Apr 1982.
- [31] Tohru Morita. Theory of Classical Fluids: Hyper-Netted Chain Approximation, I: Formulation for a One-Component System. *Progress of Theoretical Physics*, 20(6):920–938, 12 1958.
- [32] J. Chihara. The direct correlation function of inhomogeneous quantum liquids. *Journal of Physics C: Solid State Physics*, 17(10):1633–1642, apr 1984.
- [33] Jens Lindhard. On the properties of a gas of charged particles. *Dan. Vid. Selsk Mat.-Fys. Medd.*, 28:8, 1954.
- [34] Nathaniel R. Shaffer and Charles E. Starrett. Correlations between conduction electrons in dense plasmas. *arXiv*, page 1910.13505, 2019.
- [35] Gilles Chabrier. An equation of state for fully ionized hydrogen. *Journal de Physique*, 51(15):1607–1632, 1990.
- [36] Safa Kasap, Cyril Koughia, and Harry E. Ruda. *Electrical Conduction in Metals and Semiconductors, Springer Handbook of Electronic and Photonic Materials*. Springer International Publishing, 2017.
- [37] Yim T. Lee and R. M. More. An electron conductivity model for dense plasmas. *The Physics of fluids*, 27(5):1273–1286, 1984.
- [38] H. Reinholz, G. Röpke, S. Rosmej, and R. Redmer. Conductivity of warm dense matter including electron-electron collisions. *Physical Review E*, 91(4):043105, 2015.
- [39] David E. Hanson, Lee A. Collins, Joel D. Kress, and Michael P. Desjarlais. Calculations of the thermal conductivity of national ignition facility target materials at temperatures near 10 ev and densities near 10 g/cc using finite-temperature quantum molecular dynamics. *Physics of Plasmas*, 18(8), 2011.
- [40] Valentin V. Karasiev, Travis Sjostrom, James Dufty, and S. B. Trickey. Accurate homogeneous electron gas exchange-correlation free energy for local spin-density calculations. *Phys. Rev. Lett.*, 112:076403, Feb 2014.
- [41] Flavien Lambert, Vanina Recoules, Alain Decoster, Jean Clerouin, and Michael Desjarlais. On the transport coefficients of hydrogen in the inertial confinement fusion regime. *Physics of Plasmas (1994-present)*, 18(5):056306, 2011.
- [42] Michael P. Desjarlais, Christian R. Scullard, Lorin X. Benedict, Heather D. Whitley, and Ronald Redmer. Density-functional calculations of transport properties in the nondegenerate limit and the role of electron-electron scattering. *Phys. Rev. E*, 95:033203, Mar 2017.
- [43] Monica Pozzo, Chris Davies, David Gubbins, and Dario Alfè. Transport properties for liquid silicon-oxygen-iron mixtures at earth’s core conditions. *Physical Review B*, 87(1):014110, 2013.
- [44] C. E. Starrett. High-temperature electronic structure with the Korringa-Kohn-Rostoker green’s function method. *Phys. Rev. E*, 97:053205, May 2018.
- [45] N.M. Gill and C.E. Starrett. Mean-force scattering potential for calculating optical properties of dense plasmas. *High Energy Density Physics*, 31:24 – 30, 2019.
- [46] T. E. Faber and J. M. Ziman. A theory of the electrical properties of liquid metals. *The Philosophical Magazine: A Journal of Theoretical Experimental and Applied Physics*, 11(109):153–173, 1965.
- [47] A.A. Ovechkin, P.A. Loboda, and A.L. Falkov. Plasma opacity calculations using the starrett and saumon average-atom model with ion correlations. *High Energy Density Physics*, 30:29 – 40, 2019.
- [48] Georg Kresse and Jürgen Hafner. Ab initio molecular dynamics for liquid metals. *Physical Review B*, 47(1):558, 1993.
- [49] Georg Kresse and Jürgen Hafner. Ab initio molecular-dynamics simulation of the liquid-metal–amorphous-semiconductor transition in germanium. *Physical Review B*, 49(20):14251, 1994.
- [50] Georg Kresse and Jürgen Furthmüller. Efficiency of ab-initio total energy calculations for metals and semiconductors using a plane-wave basis set. *Computational materials science*, 6(1):15–50, 1996.

- [51] John P. Perdew, Kieron Burke, and Matthias Ernzerhof. Generalized gradient approximation made simple. *Phys. Rev. Lett.*, 77:3865–3868, Oct 1996.
- [52] John P. Perdew, Kieron Burke, and Matthias Ernzerhof. Generalized gradient approximation made simple [phys. rev. lett. 77, 3865 (1996)]. *Phys. Rev. Lett.*, 78:1396–1396, Feb 1997.
- [53] Peter E Blöchl. Projector augmented-wave method. *Physical review B*, 50(24):17953, 1994.
- [54] Georg Kresse and D Joubert. From ultrasoft pseudopotentials to the projector augmented-wave method. *Physical Review B*, 59(3):1758, 1999.
- [55] C. E. Starrett, R. Perriot, N. R. Shaffer, T. Nelson, L. A. Collins, and C. Ticknor. Tabular electrical conductivity for aluminum. *Contributions to Plasma Physics, in press*, 2019.